



# Three-dimensional modeling of anode-supported planar SOFC with different shapes of corrugated electrolytes

Yinghao Wang<sup>1</sup> · Genhua Su<sup>2</sup> · Zhao Li<sup>3</sup> · Debang Zhang<sup>4</sup> · Aodi Shi<sup>1</sup> · Zunlong Jin<sup>1</sup>

Received: 5 December 2022 / Revised: 16 January 2023 / Accepted: 16 January 2023 / Published online: 28 January 2023  
© The Author(s), under exclusive licence to Springer-Verlag GmbH Germany, part of Springer Nature 2023

## Abstract

This study intends to theoretically analyze the effects of different shapes of corrugated electrolytes on cell performance. On the basis of the mesoscale electrode–electrolyte interface modification theory, corrugated electrolytes with different shapes are applied to conventional anode-supported planar solid oxide fuel cells (SOFCs). Three-dimensional models of solid oxide fuel cells with electrolytes corrugated in different shapes were developed. For the purpose of further understanding the influence mechanism of the corrugated electrolyte on the cell, we analyze the influence of the corrugated electrolyte on the overall performance of the cell. Furthermore, the local gas distribution, concentration polarization, activation polarization, exchange current density and electron current density are discussed. Results indicate that the corrugated electrolyte structure reduces the local exchange current density, while the extension of the activation reaction zone results in an increase in the overall charge transfer, which leads to the improvement of cell performance. And for different corrugated shapes, the area expansion degree of corrugated electrolyte is proportional to the degree of cell performance improvement. Under the operating voltage of 0.7 V, the average current density improvement percentage of the rectangular corrugated electrolyte with a spreading factor of 1.47 is 38.01%.

**Keywords** Anode support · Corrugated electrolyte · Performance improvement · SOFC · Structure optimization

## Latin letters

$F$	Volume force vector
$\vec{u}$	Velocity vector
$x_i$	Mole fraction of the gas phase component $i$
$b_k$	Component-related parameters
$w_i$	Mass fraction of component $i$
$D_i^T$	Thermal diffusivity (in this study, it is assumed that it is zero)
$S_i$	Source term for the electrochemical reaction
$D_{ij}$	Binary diffusivity of a mixture of substances $i$ and $j$
$M_i$	Molar masses of gas components $i$
$M_j$	Molar masses of gas components $j$

$D_{K,i}$	Knudsen diffusion coefficient
$D_{\text{eff},ij}$	Effective diffusion coefficient
$d_{\text{pore}}$	Average pore size
$Q$	Heat generation/consumption
$c_p$	Gas relative heat
$k_{\text{eff}}$	Effective thermal conductivity of the porous electrode
$k_s$	Effective thermal conductivity of the solid material
$k_g$	Effective thermal conductivity of the gas
$E^{\text{OCV}}$	Equilibrium potential under operating conditions
$E_0$	Temperature-dependent open circuit voltage at standard pressure
$p_i$	Partial pressure of species $i$
$R$	Ideal gas constant
$F$	Faraday constant
$E_{\text{eq},a}$	Anodic equilibrium potentials
$E_{\text{eq},c}$	Cathodic equilibrium potentials
$C_{\text{ref}}$	Reference concentrations
$S_V$	Active surface area to volume ratio
$n_e$	Number of electrons transferred
$i_0$	Exchange current densities

✉ Zunlong Jin  
zljjin@zzu.edu.cn

<sup>1</sup> School of Mechanical and Power Engineering, Zhengzhou University, Zhengzhou 450001, China

<sup>2</sup> Henan Zhengzhou Mining Machinery CO., LTD., Zhengzhou 450122, China

<sup>3</sup> The Boiler & Pressure Vessel Safety Inspection Institute of Henan Province, Zhengzhou 450016, China

<sup>4</sup> Zhengzhou Wangu Machinery Co., LTD., Zhengzhou 450041, China

### Greek Letters

$\kappa$	Permeability of the porous medium
$\psi$	Viscous stress tensor
$\varepsilon$	Porosity of the porous material
$\rho$	Density of the gas mixture
$\mu$	Viscosity of the gas mixture
$\nu_i$	Diffusion volumes of species $i$
$\nu_j$	Diffusion volumes of species $j$
$\tau$	Tortuosity of the porous electrode
$\varphi_l$	Ion potential
$\varphi_s$	Electron potential
$\sigma_{l,\text{eff}}$	Effective conductivities of ions
$\sigma_{s,\text{eff}}$	Effective conductivities of electrons
$\varepsilon_l$	Volume fractions of ionic
$\varepsilon_s$	Volume fractions of electronically
$\sigma_l$	Ionic conductivity
$\sigma_s$	Electronic conductivity
$\eta_{\text{act}}$	Activation polarization
$\eta_{\text{ohm}}$	Ohmic polarization
$\eta_{\text{conc}}$	Concentration polarization

## Introduction

After hydropower, thermal power, and nuclear power, fuel cell technology is the fourth generation of widely used power generation technology. It is a chemical power device that continuously converts the chemical energy of fuel into electrical energy through electrochemical reactions. Among all fuel cells, solid oxide fuel cells have been widely studied and applied due to their advantages of high efficiency and fuel flexibility. At the heart of the cell is the electrolyte, a solid oxide capable of transporting ions at high temperatures, typically 600–900 °C. Due to its higher operating temperature and higher cost, its power density needs to be increased to hopefully commercialize solid oxide fuel cell technology. The power generated in a cell depends on the active area of the electrodes and is adversely influenced by activation polarization, ohmic polarization, and concentration polarization.

One of the main methods is to expand the active area of the electrode through the optimization of the structure and to enhance the overall performance of the cell under the premise of considering the adverse effects of polarization. From the perspective of geometric feature length, the structure optimization methods can be divided into three categories [1, 2] according to the feature length. The first is a macro-structural modification of the cell design, with characteristic lengths typically greater than 1 mm. The second is to optimize the cell on the microstructure, and its characteristic length is usually less than 1  $\mu\text{m}$ . By changing various parameters on the microstructure, such as porosity, volume fraction, and bending coefficient, the purpose

of effectively improving the cell performance is achieved. A third approach to improve cell power density is to optimize at a scale between the above two approaches, called mesoscale structural control, with characteristic lengths of 10–100  $\mu\text{m}$ .

A typical mesoscale structure optimization method that has been proposed is to design the electrode/electrolyte interface into a corrugated shape to form a corrugated electrolyte, which increases the three-phase boundary length by contrast with the traditional planar SOFC without changing the macrostructure, on the premise of increasing the cell's active reaction area [3]. With the development of solid oxide fuel cell structure optimization and the understanding of mesoscale structure optimization, more and more scholars have paid attention to the influence of corrugated electrolytes on fuel cells. Cebollero et al. [4] used a pulsed laser approach to conceptually modify yttria-stabilized zirconia (YSZ) electrolytes at the mesoscale to form corrugated electrolytes and experimentally demonstrated that this optimization could improve cell power density. Su et al. [5] deposited a yttria-stabilized zirconia film which is 70 nm thick on a pre-patterned silicon substrate to develop a low-temperature miniature SOFC with a corrugated electrolyte membrane. The cell performance was tested, and the study indicated that the increase of the resulting electrochemically active area increased the power output of the cell compared to the same cell with a planar membrane. Chao et al. [6] fabricated the electrolyte membrane into a corrugated shape through nanosphere lithography and atomic layer deposition methods, reducing polarization and ohmic losses at low temperatures, thereby improving cell performance.

At present, the manufacture of corrugated electrolytes requires relatively high process requirements and requires advanced manufacturing equipment and harsh experimental environments. With the advancement of technology and further research on corrugated electrolytes, the difficulty and cost of its manufacture will be reduced. At present, numerical simulation is a simple and necessary research method, which can show the specific performance parameters inside the cell; a more profound understanding of how the corrugated electrolyte improves cell performance provides theoretical guidance for subsequent experiments. Akio Konno et al. [1] conducted numerical simulations in a two-dimensional model to analyze the influence of corrugated electrolytes on various parameters inside the cell and the improvement of the overall performance of the cell. Chesnaud et al. [7] introduced three geometrically patterned corrugated electrolytes in a two-dimensional model and compared their performance with flat electrolyte cells. The performance of corrugated electrolyte cells was significantly improved. Delloro et al. [8] compared rectangular corrugated electrolytes and planar electrolytes in a two-dimensional model through steady-state finite-element simulations and proved that the former has certain advantages.

Furthermore, the study proposes that the shape of the corrugations is a subject for further study. It is mentioned that triangular ripples may be more advantageous, but it is only hypothetical and no relevant simulation research has been made. In tubular solid oxide fuel cells, the structure of the electrolyte also affects the cell performance. Otake et al. [9] investigated the relationship between the performance of micro-tubular cells and the thickness of the GDC electrolyte was examined at temperatures between 500 and 650 °C. The performance of the cell with a 15.5- $\mu\text{m}$ -thick electrolyte was higher than the cell with 40  $\mu\text{m}$  thick at lower temperatures. Jia et al. [10] proposed that decreasing the thickness of the electrolyte leads to an increase in the power output of the SOFC.

As we can see that the existing numerical simulation of corrugated electrolytes is mainly based on the two-dimensional model to analyze the cell, and it has been proven on the two-dimensional model that the existence of corrugated electrolytes improves the performance of the fuel cell. However, for the corrugated electrolyte cell. As the technology becomes more mature, we need to understand the changes in the internal working conditions of the corrugated electrolyte cell, so as to know more clearly the mechanism by which the corrugated electrolyte improves the cell performance. Therefore, more promising research and analysis of corrugated electrolytes should be simulated in 3D simulation. Second, for the further development of corrugated electrolytes, the performance changes of corrugated electrolyte cells with different shapes should be comparatively analyzed in the simulation. Based on this, this paper introduces corrugated electrolytes of different shapes into the traditional solid oxide fuel cell three-dimensional model for simulation research and analyzes the influence of corrugated electrolytes on the internal working state and the overall performance of the SOFC.

In this study, a typical planar electrolyte cell and three 3D models of corrugated electrolyte cells with different shapes were constructed for computational simulation, and the influence of distinct corrugated shapes on the cell property was studied. The model analyzes the specific changes of activation polarization, exchange current density, electron current density, gas composition distribution and concentration polarization under the premise of comprehensively considering flow, mass and heat transfer, and electrochemical phenomena. A clearer understanding of the impact mechanism of corrugated electrolytes on cell property and the influence of different shapes of corrugations on cell property are compared and studied.

## Mathematical model

### Model description

A common SOFC model consists of a porous composite anode and cathode with a dense electrolyte [11], consisting of an anode, cathode, and electrolyte in a structure called PEN. Fuel and air will diffuse to the three-phase boundary (TPB) near the electrode/electrolyte for reaction. A newly proposed five-layer PEN structure consisting of a cathode current collecting layer (CCCL), a cathode functional layer (CFL), an electrolyte, an anode functional layer (AFL), and an anode supporting layer (ASL) increases the number of reaction sites and the TPB length improves the performance of the cell [12], as shown in Fig. 1. This study is modeled on the basis of the newly proposed five-layer PEN structure.

In this study, on the basis of the commercial software COMSOL Multiphysics 5.6 ensuring that the macroscopic volume of the cell remains unchanged, a cell model with

**Fig. 1** Schematic diagram of the unit cell for an anode-supported planar SOFC

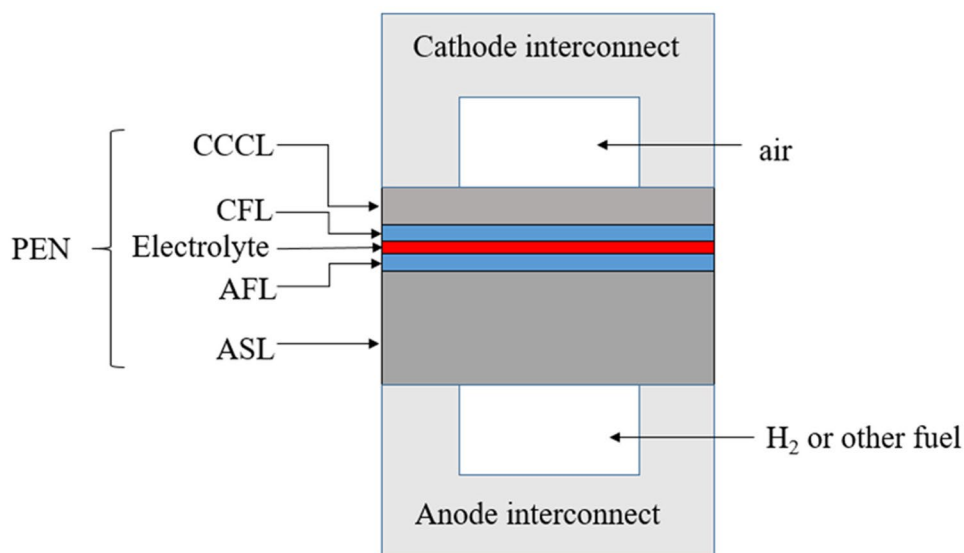
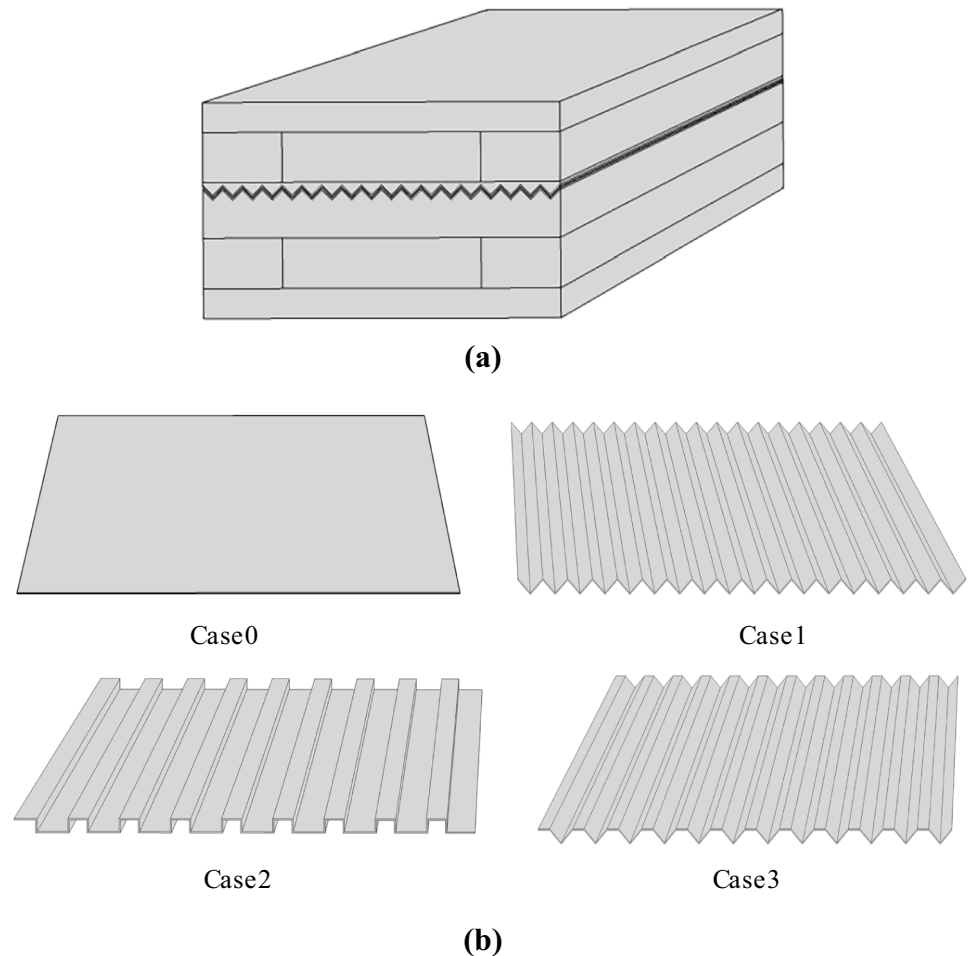


**Fig. 2** Schematic of anode-supported SOFC with corrugated electrolyte. **a** The unit cell model for SOFC with corrugated electrolyte. **b** Planar electrolyte and corrugated electrolyte



corrugated electrolytes of different shapes is established. There are triangular electrolytes, rectangular electrolytes, and mixed electrolytes. The composition of the model structure is shown in Fig. 2. Table 1 lists the distribution of each case, and Table 2 lists the detailed geometric parameters.

In the corrugated electrolyte cell, the electrolyte thickness is fixed at  $10\ \mu\text{m}$ ; although there are fluctuations in shape, we set the maximum size of the anode surface to the anode/electrolyte interface to be  $500\ \mu\text{m}$ , and the minimum size of the cathode surface to the cathode/electrolyte interface to be  $50\ \mu\text{m}$ , so the PEN thickness is the same for each corrugated electrolyte cell and the flat electrolyte cell model. It should be noted that Konno et al. [2] proposed that the characteristic length of the corrugation needs to be larger than the effective thickness of the electrode. Therefore, in order to ensure the consistency of various situations, combined with

the geometric thickness of the electrode in this model, for the three geometric electrolytes except the planar electrolyte, they are all immersed in the electrode to a depth of  $100\ \mu\text{m}$ .

### Model assumptions

In building the SOFC model, the basic assumptions and simplifications are set below:

**Table 2** Geometric parameters of the model

Parameter	Value
Cell length $L$	40 mm
PEN width $W_{\text{PEN}}$	3.6 mm
ASL thickness $H_{\text{ASL}}$	480 $\mu\text{m}$
AFL thickness $H_{\text{AFL}}$	20 $\mu\text{m}$
Electrolyte thickness $H_{\text{E}}$	10 $\mu\text{m}$
CFL thickness $H_{\text{CFL}}$	20 $\mu\text{m}$
CCCL thickness $H_{\text{CCCL}}$	30 $\mu\text{m}$
Gas flow channel width $W_{\text{CH}}$	2 mm
Gas flow channel height $H_{\text{CH}}$	0.5 mm
Interconnect thickness $H_{\text{INT}}$	0.3 mm

**Table 1** A 3D models for four cases

	Planar electrolyte	Triangular electrolyte	Rectangular electrolyte	Mixed electrolyte
Model name	Case 0	Case 1	Case 2	Case 3

1. The fuel and oxidizing gas are assumed to be ideal and incompressible.
2. The model operates under steady-state conditions and does not consider the SOFC start and stop processes.
3. The gas flow is laminar flow.
4. Electrochemical reactions take place only in functional regions.
5. The material properties of all parts in the model are uniform and isotropic.
6. Radiation heat transfer and contact resistance between components are ignored.

## Governing equations

Modeling of SOFC involves coupled phenomena of fluid flow, mass and heat transfer, charge transfer, and electrochemical reactions. Because many physical quantities are involved in the actual situation, the equation in the model is simplified. The following describes the equations used in this study.

## Momentum transport

In the simulation of this study, flow rate and pressure changes of free flow in gas channel and gas flow in porous electrodes need to be studied, so momentum transfer should be included in the equation solved. The governing equation for momentum transfer uses the Brinkman equation, because it solves the boundary conditions at the interface between the gas channel and the porous medium. Equation (1) enables continuous velocity and pressure fields, i.e., channels and porous regions are treated as a single domain [13].

$$\left(\frac{\mu}{\kappa} + \rho \cdot \nabla \cdot \vec{u}\right) \cdot \vec{u} - \nabla \left[-\rho + \frac{1}{\varepsilon} \left\{ \Psi - \left(\frac{-2}{3} \cdot \mu\right) (\nabla \cdot \vec{u}) \right\}\right] = F \quad (1)$$

where  $F$  is the volume force vector,  $\kappa$  is the permeability of the porous medium,  $\vec{u}$  is the velocity vector,  $\psi$  is the viscous stress tensor, and  $\varepsilon$  is the porosity of the porous material.

When the porosity and permeability terms in Eq. (1) are removed, the simplified momentum equation for the gas channel is shown below:

$$\rho \cdot (\nabla \cdot \vec{u}) \cdot \vec{u} - \nabla \left[-p + \mu \cdot \left\{ \psi - \frac{2}{3} \cdot (\nabla \cdot \vec{u}) \right\}\right] = F \quad (2)$$

The density  $\rho$  and viscosity  $\mu$  of the gas mixture depend on the temperature and mole fraction [14].

$$\rho_g = \frac{p}{RT} \left( \sum_i x_i M_i \right) \quad (3)$$

$$\mu_i = \sum_{k=0}^6 b_k \cdot \left(\frac{T}{1000}\right)^k \quad (4)$$

$$\mu_g = \sum_i x_i \cdot \mu_i \quad (5)$$

Among them,  $x_i$  and  $\mu_i$  figure the mole fraction and viscosity of the gas phase component  $i$ , respectively,  $\mu_g$  represents the dynamic viscosity of the mixed gas, and  $b_k$  represents the component-related parameters.

## Mass transport

The following is a description of the steady-state mass balance in the fuel and air channels and porous electrodes [15]:

$$\left(-\rho \cdot w_i \sum^n D_{eff,if} \cdot \nabla x_j + (x_j - w_j) \frac{\nabla p}{p} \vec{u} - D_i^T \cdot \frac{\nabla T}{T}\right) + \rho \cdot \vec{u} \cdot \nabla w_j = S_i \quad (6)$$

where  $w_i$  is the mass fraction of component  $i$ ,  $D_i^T$  is the thermal diffusivity (in this study, it is assumed that it is zero), and  $S_i$  is the source term for the electrochemical reaction.

$D_{ij}$  is the binary diffusivity of a mixture of substances  $i$  and  $j$  calculated as follows [16]:

$$D_{ij} = \frac{3.198 \times 10^{-8} \sigma^{1.75}}{P \left(v_i^{1/3} + v_j^{1/3}\right)} \left(\frac{1}{M_i} + \frac{1}{M_j}\right)^{0.5} \quad (7)$$

where  $\nu_i$  and  $\nu_j$  are the diffusion volumes of species  $i$  and  $j$ , respectively.  $M_i$  and  $M_j$  are the molar masses of gas components  $i$  and  $j$ , respectively.

The combined effect of molecular diffusion and Nussen diffusion in porous electrodes is considered in this study. The Knudsen diffusion coefficient  $D_{K,i}$  can be calculated from Eq. (8) and the effective diffusion coefficient  $D_{eff,ij}$  can be calculated from Eq. (9) [17]:

$$D_{K,i} = \frac{d_{pore}}{3} \left(\frac{8RT}{\pi M_i}\right)^{0.5} \quad (8)$$

$$D_{eff,if} = \frac{\varepsilon}{\tau} \frac{D_{ij} D_{K,i}}{D_{ij} + D_{K,i}} \quad (9)$$

where  $d_{pore}$  is the average pore size and  $\tau$  is the tortuosity of the porous electrode.

## Heat transport

Heat transfer kinetics involves the generation, transfer, and consumption of heat and various heat transfer mechanisms. This study employs a local temperature equilibrium

approach, which assumes that the temperatures of the solid and gas phases in the porous electrode are locally the same. The steady-state energy conservation equation is as follows:

$$\rho_g \cdot c_{p,g} \cdot \vec{u} \cdot \nabla T = \nabla \cdot (k_{\text{eff}} \nabla T) + Q \quad (10)$$

where  $Q$  is the heat generation/consumption,  $c_p$  is the gas relative heat, and  $k_{\text{eff}}$  is the effective thermal conductivity of the porous electrode [15].

$$k_{\text{eff}} = \varepsilon k_g + (1 - \varepsilon) k_s \quad (11)$$

where  $k_s$  is the thermal conductivity of the solid material and  $k_g$  is the effective thermal conductivity of the gas.

Calculations of specific heat and thermal conductivity of various gases and gas mixtures are listed below [14]:

$$c_{p,i} = \sum_{k=0}^6 a_k \cdot \left(\frac{T}{1000}\right)^k \quad (12)$$

$$c_{p,g} = \sum x_i \cdot c_{p,i} \quad (13)$$

$$k_i = 0.01 \cdot \sum_{k=0}^6 c_k \cdot \left(\frac{T}{1000}\right)^k \quad (14)$$

$$k_g = \sum_i x_i \cdot k_i \quad (15)$$

where  $a_k$  and  $c_k$  are decided by the physical properties of the gas and can be extracted from experimental results [14].

### Charge transport and electrochemical reactions

In this study, the fuel in the anode is hydrogen and the oxidizer in the cathode is air. The oxidation reaction of  $\text{H}_2$  releases a pair of electrons and forms  $\text{H}_2\text{O}$ .  $\text{O}_2$  is reduced to form oxygen ions. The electrochemical reaction equations in the electrode are shown in Eqs. (16) and (17).



Charge transfer comprises electron transfer and ion transfer. In ASL, CCCL, and interconnects, only electrons are conductive particles. In both AFL and CFL, conductive particles have electrons and ions. The governing equations for electron and ion transport are shown below.

$$i_l = \nabla \cdot (-\sigma_{l,\text{eff}} \nabla \varphi_l) \quad (18)$$

$$i_s = \nabla \cdot (-\sigma_{s,\text{eff}} \nabla \varphi_s) \quad (19)$$

where  $\varphi_l$  and  $\varphi_s$  are the ion potential and electron potential;  $\sigma_{l,\text{eff}}$  and  $\sigma_{s,\text{eff}}$  are the effective conductivities of ions and electrons.

In addition to the inherent properties of the electrode material, the microstructure of the porous electrode also affects the effective conductivity of the electrode. The effective conductivity can be expressed as [18]:

$$\sigma_{l,\text{eff}} = \sigma_l \cdot \frac{\varepsilon_l}{\tau} \quad (20)$$

$$\sigma_{s,\text{eff}} = \sigma_s \cdot \frac{\varepsilon_s}{\tau} \quad (21)$$

where  $\varepsilon_l$  and  $\varepsilon_s$  are the volume fractions of ionic and electronically conductive particles in the porous electrode, and  $\sigma_l$  and  $\sigma_s$  are the ionic and electronic conductivity.

SOFC has the internal resistance and polarization losses; under operating conditions, the actual output voltage  $V_{\text{cell}}$  is lower than the ideal equilibrium potential all the time. The actual output voltage can be described as:

$$V_{\text{cell}} = E^{\text{OCV}} - (\eta_{\text{act}} + \eta_{\text{ohm}} + \eta_{\text{conc}}) \quad (22)$$

where  $\eta_{\text{act}}$  is the activation polarization,  $\eta_{\text{ohm}}$  is the ohmic polarization, and  $\eta_{\text{conc}}$  is the concentration polarization.  $E^{\text{OCV}}$  is the equilibrium potential under operating conditions. Nernst equation can calculate  $E^{\text{OCV}}$  [19].

$$E^{\text{OCV}} = E_0 - \frac{R \cdot T}{2 \cdot F} \cdot \ln \left( \frac{P_{\text{H}_2\text{O}}}{P_{\text{H}_2} \sqrt{P_{\text{O}_2}}} \right) \quad (23)$$

$$E_0 = 1.253 - 2.4516 \times 10^{-4} \cdot T \quad (24)$$

where  $E_0$  is the temperature-dependent open circuit voltage at standard pressure,  $p_i$  is the partial pressure of species  $i$ ,  $R$  is the ideal gas constant, and  $F$  is the Faraday constant.

The activation polarization of the anode and cathode can be defined as:

$$\eta_{\text{act},a} = (\varphi_s - \varphi_l) - E_{\text{eq},a} \quad (25)$$

$$\eta_{\text{act},c} = (\varphi_s - \varphi_l) - E_{\text{eq},c} \quad (26)$$

$E_{\text{eq},a}$  and  $E_{\text{eq},c}$  represent the anodic and cathodic equilibrium potentials, which can be expressed by the following expressions [20]:

$$E_{\text{eq},a} = \frac{RT}{2F} \ln \frac{P_{\text{H}_2\text{O}}}{P_{\text{H}_2}} \quad (27)$$

**Table 3** Solid material parameters

	Anode (Ni YSZ)	Cathode (LSM-YSZ)	Electrolyte (YSZ)	Interconnect (stainless steel)
Density (kg·m <sup>-3</sup> )	3310	3030	5160	3030
Specific heat (J·kg <sup>-1</sup> ·K)	450	430	470	550
Thermal conductivity (W·m <sup>-1</sup> ·K)	11	6	2.7	20

$$E_{eq,c} = E_0 + \frac{RT}{4F} \ln \frac{p_{O_2}}{p_0} \tag{28}$$

The Butler-Volmer equation can calculate Bulk current density due to charge transfer. This paper uses the concentration-dependent kinetic equation to calculate the local exchange current density [21].

$$i_a = S_V i_{0,a} \left[ \frac{C_{H_2}}{C_{H_2,ref}} \exp\left(\frac{n_e \alpha_a F}{RT} \eta_{act,a}\right) - \frac{C_{H_2O}}{C_{H_2O,ref}} \exp\left(\frac{-n_e \beta_a F}{RT} \eta_{act,a}\right) \right] \tag{29}$$

$$i_c = S_V i_{0,c} \left[ \exp\left(\frac{n_e \alpha_c F}{RT} \eta_{act,c}\right) - \frac{C_{O_2}}{C_{O_2,ref}} \exp\left(\frac{-n_e \beta_c F}{RT} \eta_{act,c}\right) \right] \tag{30}$$

Among them,  $C_{H_2,ref}$ ,  $C_{H_2O,ref}$  and  $C_{O_2,ref}$  are the reference concentrations of hydrogen, water and oxygen,  $S_V$  is the active surface area to volume ratio, which can be understood as the contact area between ionic and electronically conducting particles per unit volume.  $S_V$  is determined by particle distribution, particle radius, particle coordination number, and even particle contact angle (ionically conductive particles: YSZ, electronically conductive particles: Ni and LSM) [22].  $n_e$  is the number of electrons transferred per reaction. Symmetrical electron transfer is usually assumed in Butler-Volmer (i.e.,  $\alpha_a = \beta_a = 0.5$ ,

$\alpha_c = \beta_c = 0.5$ ) [23].  $i_{0,a}$  and  $i_{0,c}$  are the exchange current densities, which can be expressed by Eqs. (31) and (32) [24].

$$i_{0,a} = \gamma^A \left(\frac{p_{H_2}}{p_0}\right) \left(\frac{p_{H_2O}}{p_0}\right) \exp\left(-\frac{E_A}{RT}\right) \tag{31}$$

$$i_{0,c} = \gamma^C \left(\frac{p_{O_2}}{p_0}\right)^{0.25} \exp\left(-\frac{E_C}{RT}\right) \tag{32}$$

Table 3 and Table 4 list the cell materials and additional relevant parameters [24–28].

### Boundary conditions

Solving the governing equations requires corresponding boundary conditions, the model used in this study is simplified according to the actual SOFC, and the following boundary conditions and assumptions are set:

1. The values of temperature, flow rate, and composition at the gas channel inlet of the electrode are constant. Fuel and air countercurrent flow in the channels.
2. The pressure at the channel outlet boundary is standard atmospheric pressure, and the airflow at the channel wall adopts the no-slip condition.

**Table 4** Other related parameters used in the present model

Parameters	Value
Volume fraction of YSZ in AFL	0.42
Volume fraction of Ni in AFL	0.28
Volume fraction of YSZ in CFL	0.42
Volume fraction of LSM in CFL	0.28
Porosity of ASL and CCCL	0.5
Conductivity of electron-conducting particles in anode (S·m <sup>-1</sup> )	$\frac{9.5 \times 10^7}{T} \exp\left(\frac{-1150}{T}\right)$
Conductivity of electron-conducting particles in cathode (S·m <sup>-1</sup> )	$\frac{4.2 \times 10^7}{T} \exp\left(\frac{-1200}{T}\right)$
Conductivity of ion-conducting particles (S·m <sup>-1</sup> )	$3.34 \times 10^4 \exp\left(\frac{-10300}{T}\right)$
Tortuosity factors	2.75
Anode pre-exponential coefficient (A·m <sup>-2</sup> )	$1.344 \times 10^{10}$
Anode activation energy (J·mol <sup>-1</sup> )	$1.0 \times 10^5$
Cathode pre-exponential coefficient (A·m <sup>-2</sup> )	$2.051 \times 10^9$
Cathode activation energy (J·mol <sup>-1</sup> )	$1.2 \times 10^5$

- Assuming that the individual cells in the study are duplicate cells in the stack.
- The wall whose heat flux density is 0 is the adiabatic surface.

Table 5 lists some of the remaining boundary conditions.

## Model validation

When building the model, we made some legitimate assumptions according to the real situation. Therefore, so as to ensure the accurateness of the research, the model needs to be verified. In actual experimental studies, SOFCs with more corrugated electrolytes are coin cells [29, 30]. However, the test conditions of coin cells are not the same as those of regular planar SOFCs, so a representative conventional anode-supported planar electrolyte SOFC was selected as the basic model in this study. Previous numerical simulations and experiments on performance comparison of corrugated electrolyte cells and planar electrolyte cells, materials, and operating parameters of the cells remain unchanged. Except for the change in electrolyte structure, the electrochemical reactions and charge transfer mechanisms of the cell remain unchanged. Thus, the model in this study can theoretically correctly represent the performance of corrugated electrolyte SOFCs.

The simulated I–V characteristic curve are in contrast with the experimental results of Li et al. [31]. To undertake the accuracy of the verification, the model material, structure, and operating parameters in the study are in agreement with the experiments. The modeling results are in contrast with the experimental results, as shown in Fig. 3. The simulated results at different current densities are consistent with the experiments under the operating conditions of 750 °C and atmospheric pressure. The specific error between numerical

simulation results and experimental results is shown in Fig. 3, and the error range shall not exceed 5%, which demonstrates the correctness of the numerical simulation calculation method in this study. The error between the simulation results and the experimental results is mainly due to the measurement error in the experiment and the model makes some assumptions that it is operating under ideal conditions [27]. In conclusion, the cell model established in this study is valid.

## Results and discussion

The effects of different shapes of corrugated electrolytes on cell performance are studied, aiming to provide guidance for the optimization of corrugated electrolytes under the meso-scale concept. The following is a theoretical analysis of the influence of SOFC on performance after numerical simulation of SOFC with different shapes of corrugated electrolytes.

The influence of corrugated electrolytes with different geometries on the volume exchange current at the anode/electrolyte interface. The Fig. 4 shows the volume exchange current at the anode/electrolyte interface for corrugated electrolyte cells with different shapes when  $V_{\text{cell}} = 0.7$  V. The calculation formula of the current density adopts the concentration-dependent kinetic equation, so the gas concentration and activation polarization have a great influence on the volume exchange current density. As can be seen from the figure that at the fuel inlet, the volume exchange current density has a maximum value and then decreases along the flow direction. Because the presence of fuel channels and connectors affect the gas transport and distribution, there is a large gradient difference in volumetric current density in the y-direction. At the anode/electrolyte interface, the maximum value for case 0 is 2.63 times the minimum value, while the maximum value for case 2 is 25.57 times the minimum value.

**Table 5** Boundary conditions

Boundary	Condition	Value
Top wall of cathode interconnect	Output cell voltage	$V_{\text{cell}}$
Bottom wall of anode interconnect	Ground potential	0
Fuel inlet	Mole fraction	21% O <sub>2</sub> + 79% N <sub>2</sub>
Air inlet	Velocity	0.5 ms <sup>-1</sup>
	Temperature	1023 K
	Mole fraction	97% H <sub>2</sub> + 3% H <sub>2</sub> O
	Velocity	3 ms <sup>-1</sup>
	Temperature	1023 K
Fuel outlet	Pressure	0
Air outlet	Pressure	0

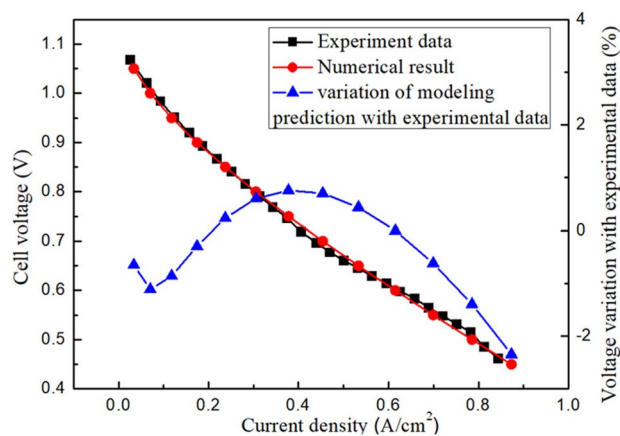


**Fig. 3** Comparison of modeling predictions with experimental data<sup>30</sup> for SOFC operated at 1023 K



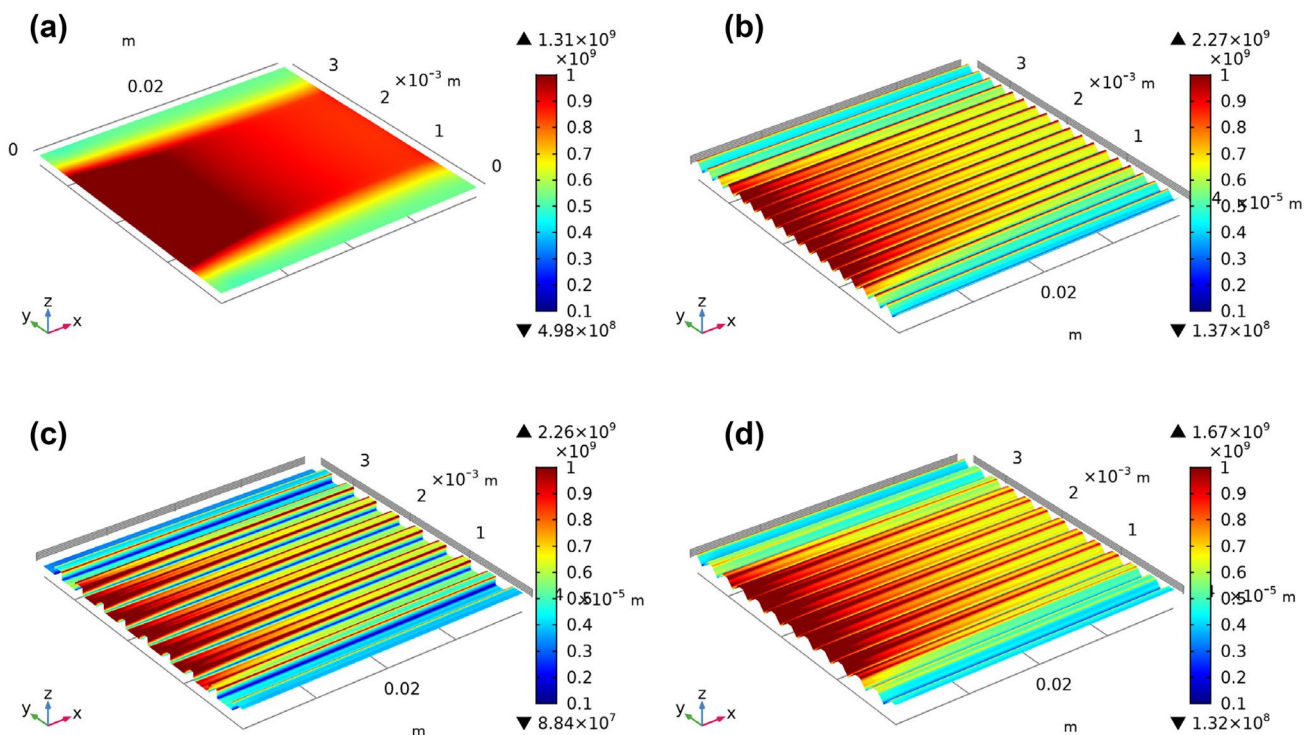


**Fig. 4** Distribution of the volume exchange current at the anode/electrolyte interface ( $A \cdot m^{-3}$ ). **a** Case 0. **b** Case 1. **c** Case 2. **d** Case 3

Figure 5 shows the average volume exchange current curves of the active reaction zone of corrugated electrolyte cells with different shapes. Since the precondition of this study assumes that the thickness of the cathodic reaction zone and the anodic reaction zone are the same, this study only analyzes the average volume exchange current density of the anode. The figure clearly shows that compared with the flat electrolyte cell of the control group, after the introduction of the corrugated electrolyte, the average volume exchange current value of the rectangular corrugated electrolyte decreases with the same corrugation height, while the corrugated electrolyte of other shapes decreases. The average volume exchange current value has increased. The reduction of the average volume exchange current of the rectangular corrugated electrolyte cell is because the introduction of the corrugated structure results in an increase in the active reaction area, so the average charge per unit volume is reduced. Liu et al. [32] demonstrated that an increase in the ripple period leads to an increase in the average volume exchange current density. Therefore, although other shapes of corrugated electrolyte cells also increase the active reaction area, their average volume exchange current is generally increased, because the increase in the average volume exchange current density caused by the increase of the cycle in this case is higher than that caused by the corrugated electrolyte. The reduction in the average volume exchange current density caused by the increase of the active reaction

zone has a greater effect. It is worth noting that although the introduction of the corrugated electrolyte may lead to a decrease in the average volume exchange current of the active reaction zone, the area of the active reaction zone is also increased because of the corrugated electrolyte. So, overall, the cell performance is still improving, which is the most important. Therefore, the introduction of a corrugated

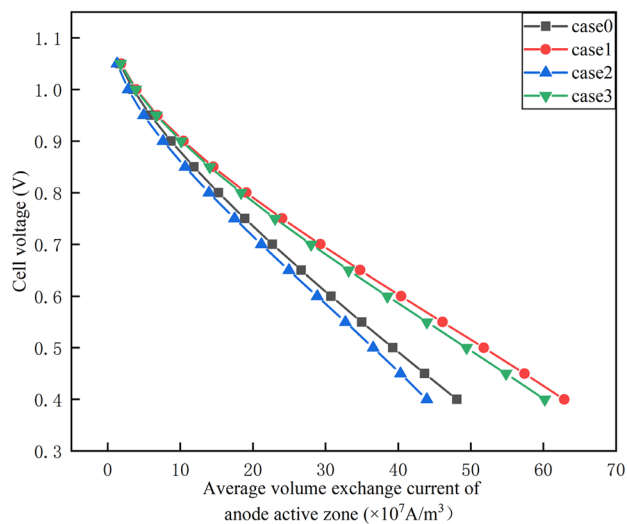


**Fig. 5** Average volume exchange current of the anode activation zone

electrolyte increases the active reaction area, thereby increasing the volume exchange current.

The influence of corrugated electrolytes with different geometries on the local electron current density distribution, as shown in the Fig. 6, when  $V_{\text{cell}} = 0.7$  V, local electron current density distribution across the cross section at  $x = 0$  mm. The small red arrow in the figure indicates the direction of current flow in the cell from anode to cathode. According to the picture, we can see that both the maximum and minimum electron current density of the cells incorporating the corrugated electrolyte is enhanced compared to the control cells with the flat electrolyte. The electron current density has a maximum at the corners of the cathode connector. Anode maxima also appear in the corners of the anode connector, but their values are small compared to the cathode maxima. This situation occurs in both flat-electrolyte and corrugated-electrolyte cells. This is because the ratio of the air channel width to the thickness of the cathode is relatively large, therefore the electron transport path in the cathode is relatively short relative to the anode, which reduces the resistance of electron transport in the cathode.

According to the picture, we can see that the electron current densities of different corrugated electrolytes are also quite different. According to the cloud diagram, we can see

that the electron current density in the cell with the triangular corrugated electrolyte is generally smaller than that of the other two shapes of corrugated electrolyte cells. This is because under the premise of the same air channel width to cathode thickness ratio, the number of corrugations in the triangular corrugated electrolyte increases, which leads to an increase in the distance of electron transfer and the resistance of electron transfer, so the overall electron current density decreases slightly.

The influence of corrugated electrolytes with different geometries on the gas distribution is shown in the figure showing the mole fractions of hydrogen and oxygen in the cross section at  $x = 20$  mm when  $V_{\text{cell}} = 0.7$  V. There are two important reasons that affect the distribution of gas in the electrode. One is that the increase or reduction of the local exchange current density near the interface will lead to an increase or a smaller amount of gas consumption; Second, the geometrical structure will determine the path of gas transportation and then affect the final distribution of gas.

According to Fig. 7, we can see that the different shapes of corrugated electrolytes have a great influence on the gas distribution compared with flat electrolytes. The introduction of corrugated electrolytes improves the utilization ratio of cathode oxygen and anode hydrogen. Consequently, compared with case 0 the hydrogen mole fraction in cases 1, 2,

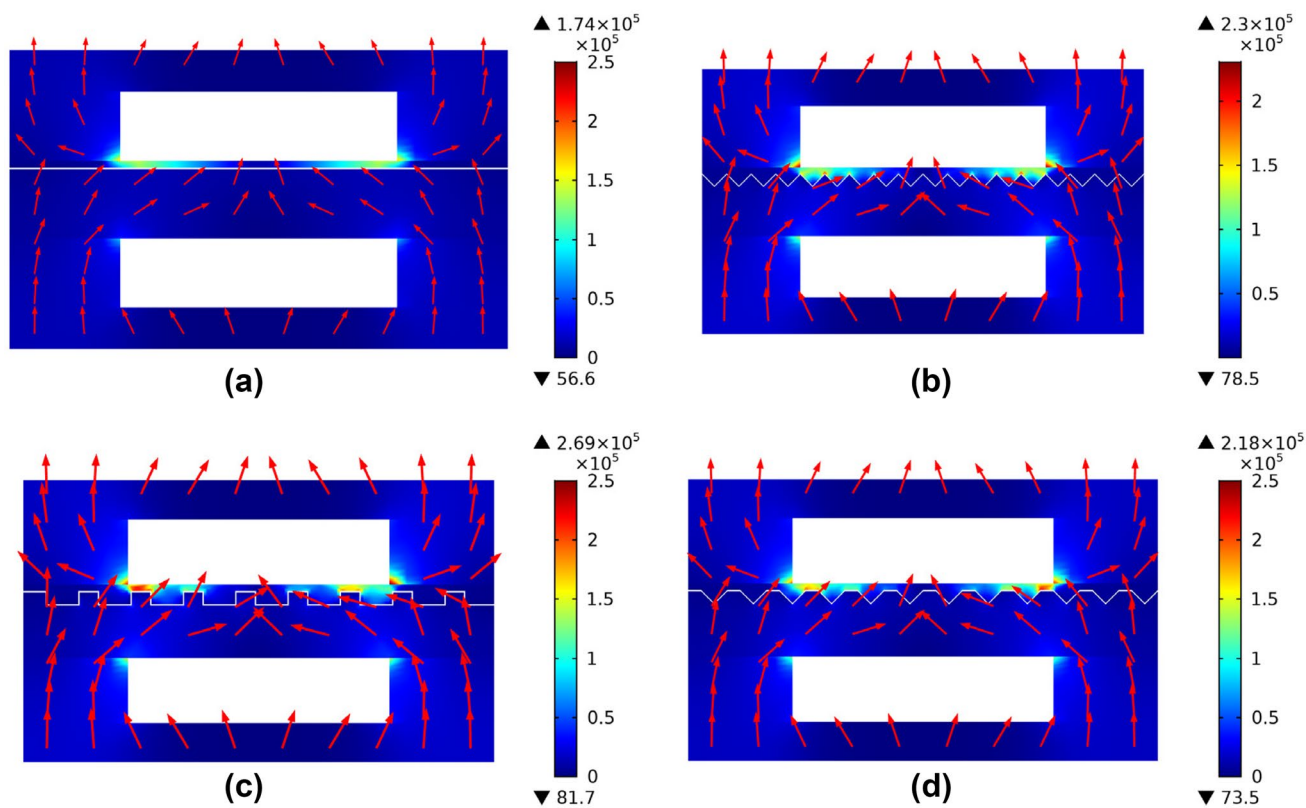


**Fig. 6** Distribution of electron current density in the cross section of  $x = 0$  ( $\text{A}\cdot\text{m}^{-2}$ ). **a** Case 0. **b** Case 1. **c** Case 2. **d** Case 3

and 3 are higher. Especially in case 2, the rectangular corrugated electrolyte has the lowest hydrogen mole fraction, that is, more hydrogen is consumed. As shown in Fig. 7b, the simulation results of different ripple conditions show that the oxygen mole fraction distribution is similar in the four cases due to excessive air entering the cathode. Because of the interconnects, the gas mole fraction under the interconnection ribs decreases obviously, compared with that under the gas channels. This is especially true in cathodes where the thinner cathode is not conducive to oxygen transfer and where oxygen is consumed by electrode reactions below the gas channel, oxygen does not diffuse easily to the electrodes below the ribs.

The influence of corrugated electrolytes with different geometries on the concentration polarization, as shown in Fig. 8, shows the concentration polarization in the  $y$ - $z$  plane of the cell at  $x = 20$  mm when  $V_{\text{cell}} = 0.7$  V. According to Fig. 8, we can see that the specific situation of concentration polarization in the thickness direction and the distribution of gas species seriously affects the concentration polarization. The study found that the concentration polarization of the electrodes at different positions is very different. In the electrode below the gas channel, the concentration polarization is very low, while in the electrode below the rib, the concentration polarization is very significant. In the horizontal direction, because the connector affects the diffusion of hydrogen and oxygen, the electrode has an obvious concentration polarization gradient. Looking vertically, the anode has an obvious concentration polarization gradient because it is thick. Compared with the anode, the cathode is very thin, so there is no obvious concentration polarization change. Comparing case 0 with cases 1, 2, and 3, it can be seen that compared with the flat electrolyte cell, the corrugated electrolyte cell exhibits a higher concentration polarization in the electrode; this is because the corrugated electrolyte increases the reaction area; more electrochemical reactions take place, consuming more hydrogen and oxygen. Negative influences caused by increased concentration polarization of cell are offset by the positive effect of the increased electrochemical reaction area caused by the corrugated electrolyte.

Figure 9 shows the average concentration polarization of the electrode/electrolyte interface. From the data in the figure, we can quantitatively analyze the change of the concentration polarization after introducing the corrugated electrolyte compared to the flat electrolyte cell. When the terminal voltage is 0.7 V, the average concentration polarization values of the corrugated electrolytes with different shapes are mostly higher than that of flat electrolytes in the control group. Case 2 had the largest improvement in the average value of anode/electrolyte by 12.61%. Case 2 had the largest improvement in the average value of cathode/electrolyte, which was 4.37% higher.

The influence of corrugated electrolytes with different geometries on the activation polarization was investigated. The activation polarization of the cell at different conditions when  $V = 0.7$  V is shown in Figs. 10 and 11 shows the average activation polarization at the electrode/electrolyte interface under different conditions. The electrochemical reactions occur mainly near the electrolyte, and therefore the activation polarization is also centered near the electrolyte. According to Eqs. (3) and (4), the activation polarization is related to the electronic potential, ionic potential, and equilibrium potential of the cell. The maximum and minimum values of activation polarization at the anode/electrolyte interface of the planar electrolyte cell of case 0 are 0.16 V and 0.09 V, respectively; the maximum and minimum values of the corrugated electrolyte cell in the triangle of Case 1 are 0.19 V and 0.06 V, respectively. Similarly, the maximum and minimum values of activation polarization at the cathode/electrolyte interface of the planar electrolyte cell of case 0 are 0.24 V and 0.13 V, respectively, and the maximum and minimum values of the triangular-shaped corrugated electrolyte cell are 0.28 V and 0.09 V in case 1, respectively. What's more, the average activation polarization at the electrode/electrolyte for cells with corrugated electrolytes is smaller than for cells with planar electrolytes of the control group, which is a positive impact of corrugated electrolytes on cell property (Fig. 11). As shown in the figure, the activation polarization in the cathode is slightly higher than the activation polarization in the anode, and by comparing the maximum reduction ratios of the activation polarization of the cathode and anode to 8.54% and 2.34% by comparing the corrugated electrolyte, it can be concluded that the ripple of the electrolyte has a greater effect on the activation polarization of the cathode. As shown in Fig. 10, in the corrugated electrolyte cell, the maximum activation polarization at the anode/electrolyte interface and the cathode/electrolyte interface occurs at the corrugated convex and concave corners, respectively. It is the presence of the corrugated electrolyte that results in a prominent ridge on the electrode where there is a higher activation polarization.

The effects of corrugated electrolytes with different geometries on the  $I$ - $V$  characteristic curves are shown in Fig. 12 for various structures. As shown in Fig. 12, at the same voltage, the average current density of the cell with corrugated electrolyte is improved compared with the cell with flat electrolyte, and the overall power generation performance of the cell with rectangular corrugated electrolyte is improved the most. Compared to cells with a flat electrolyte, the voltage of cells with a corrugated electrolyte increases compared to cells with a flat electrolyte at a constant current density, which indicates that the total polarization loss of the cell decreases with the introduction of the corrugated electrolyte.

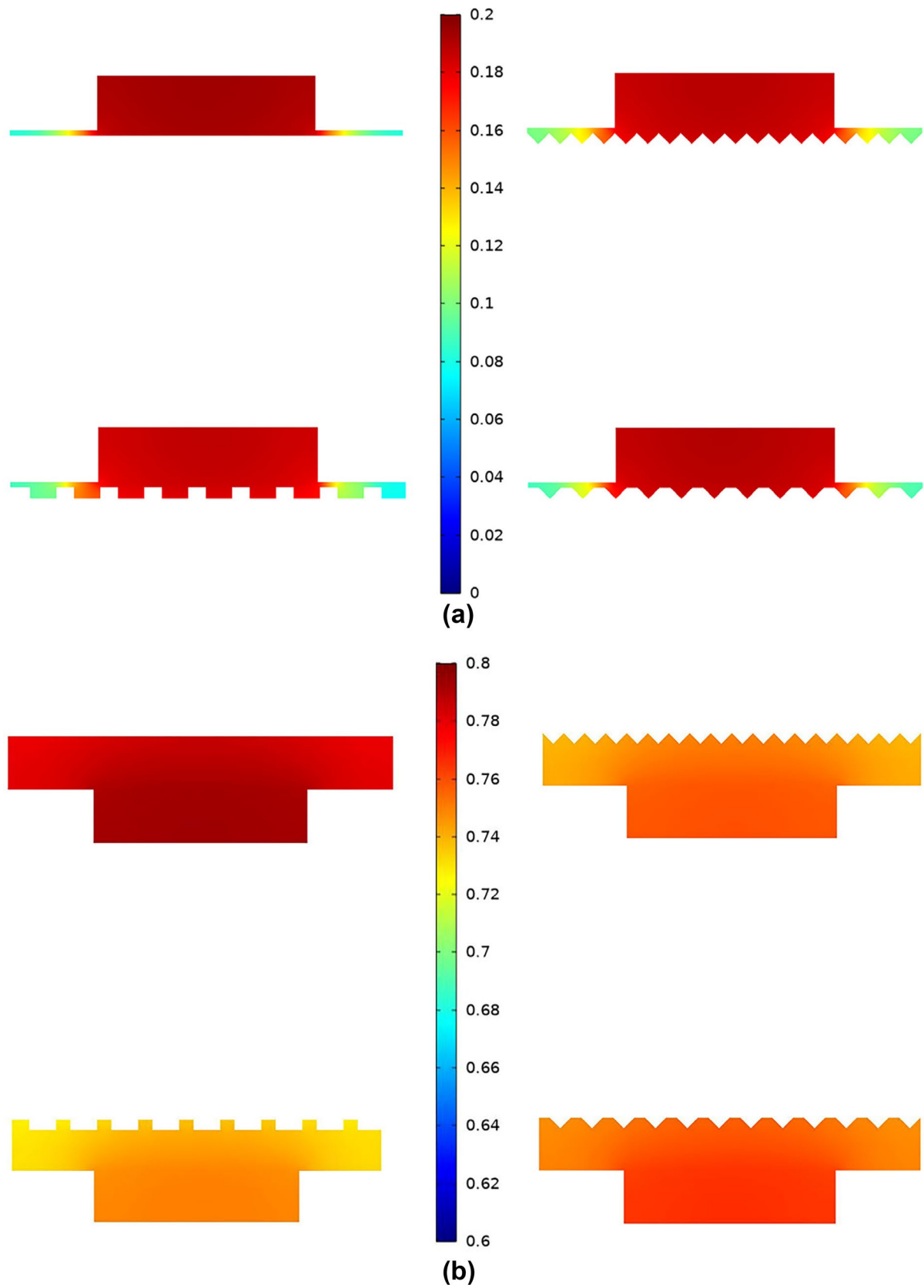


**Fig. 7**  $H_2$  and  $O_2$  mole fraction distribution on  $x=20$  mm cross section. **a** Cathode,  $V_{cell}=0.7$  V. **b** Anode,  $V_{cell}=0.7$  V

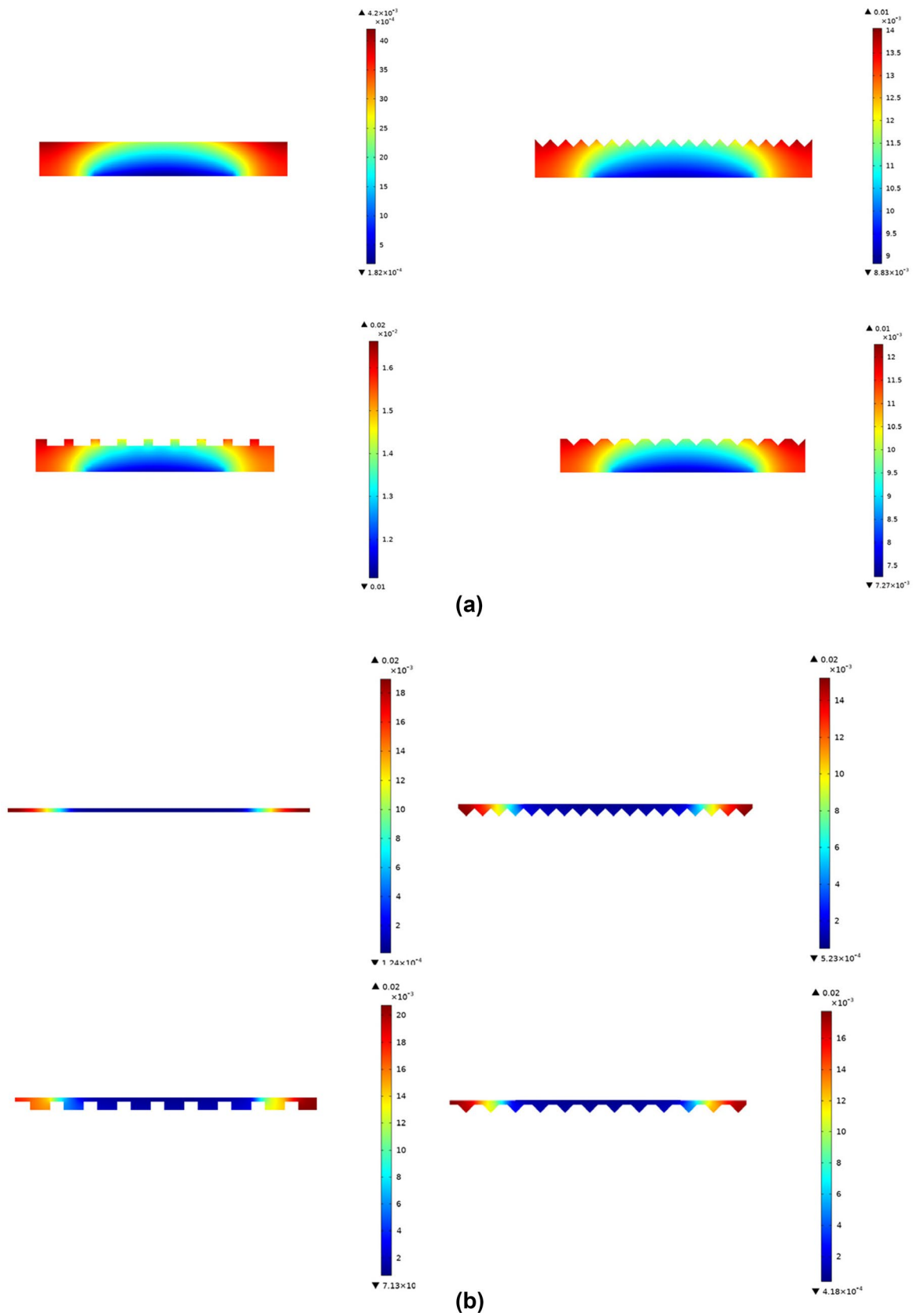
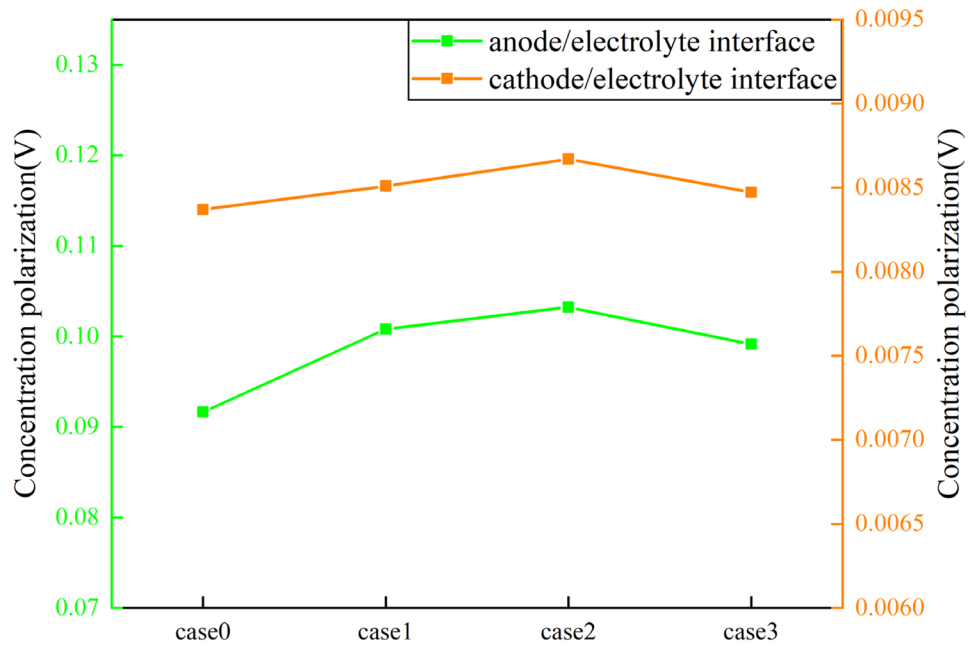


**Fig. 8** Concentration polarization distribution in the cross section of  $x=20$  mm at  $V_{\text{cell}}=0.7$  V. **a** Anode. **b** Cathode

**Fig. 9** Average concentration polarization at the electrode/electrolyte interface at a terminal voltage of 0.7 V



$$\lambda = \frac{S_{\text{corrugated electrolyte}}}{S_{\text{planar electrolyte}}} \quad (33)$$

A new coefficient,  $\lambda$  (expansion coefficient), is set here to more clearly analyze the effect of introducing a corrugated electrolyte on the overall cell performance. The expansion factor is

defined as the ratio of the surface area of the corrugated electrolyte to the surface area of the flat electrolyte, as shown in Eq. (33). On this basis, in this study, the relationship between the enhancement of current density, the ripple shape of the corrugated electrolyte and the expansion coefficient  $\lambda$  at a typical operating voltage of 0.7 V was deliberately analyzed. Table 6 lists the  $\lambda$  value and current density expansion percentage for

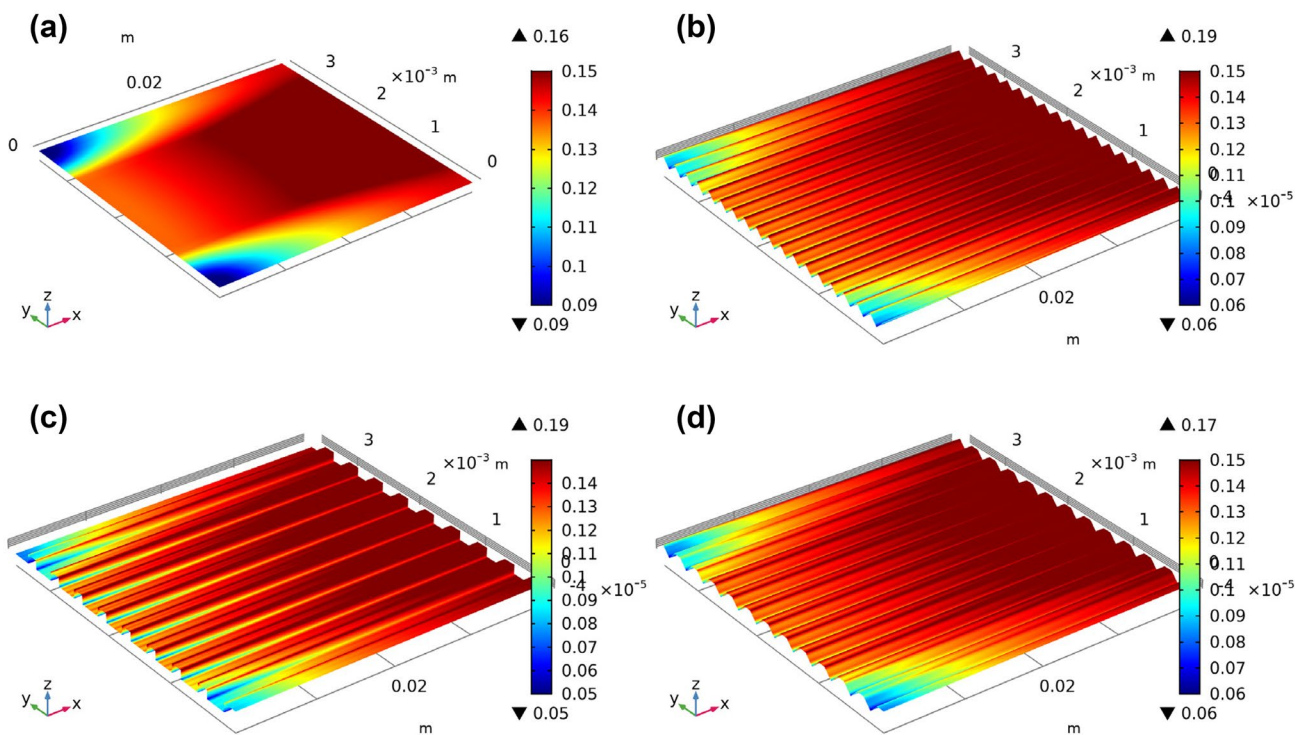


**Fig. 10** Activation polarization at the anode/electrolyte interface. **a** Case 0. **b** Case 1. **c** Case 2. **d** Case 3

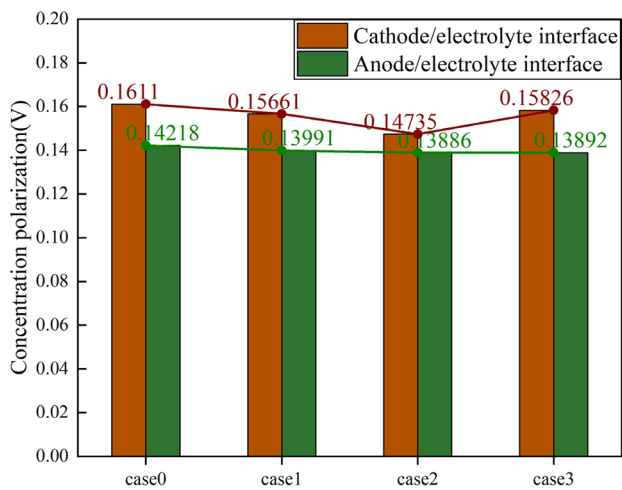


**Fig. 11** Average activation polarization at the electrode/electrolyte interface for all cases at 0.7 V

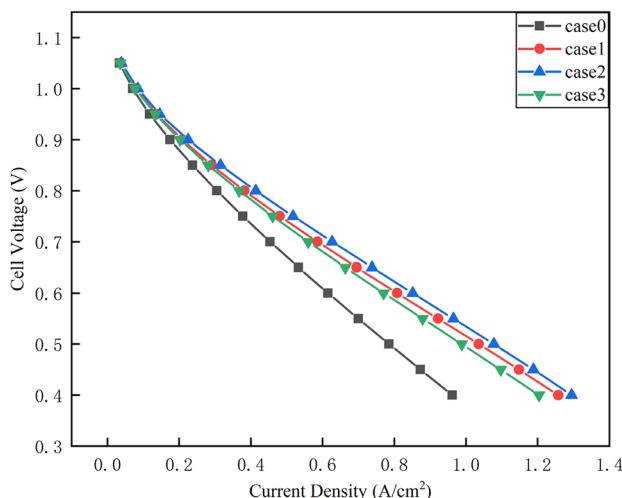


**Fig. 12** I–V characteristic curve for each case

each case at  $V_{cell}=0.7$  V. It can be seen from the table that when  $V_{cell}=0.7$  V, the current density of the rectangular corrugated electrolyte cell with the largest  $\lambda$  value is the highest, which is 38.01%. It can be seen that the area expansion degree of the corrugated electrolyte is proportional to the improvement of the cell performance, which provides a certain reference for the subsequent research on the corrugated electrolyte.

**Table 6**  $\lambda$  value and current density expansion percentage at  $V_{cell}=0.7$  V

	Case 0	Case 1	Case 2	Case 3
$\lambda$	1	1.414	1.47	1.28
Expansion percentage		29.02%	38.01%	23.39%

## Conclusions

In this study, three simple corrugated electrolyte solid oxide fuel cells were established, namely triangular, rectangular, and hybrid shapes. By means of numerical simulation, its performance is compared with that of the solid oxide fuel cell with a planar electrolyte in the control group. The effect of corrugated electrolytes on cell parameters and performance was investigated. The conclusions are as follows:

1. The average volume exchange current density of the rectangular corrugated electrolyte cell is lower than that of the flat electrolyte cell, but the average volume exchange current density of the triangular and hybrid type is higher than that of the flat electrolyte cell due to the increase of the corrugation period, but the output of the three corrugated electrolyte cells is higher than that of the flat electrolyte cell. The performance is higher than that of planar electrolyte cells. This is because the existence of the corrugated electrolyte enlarges the active reaction area without changing the macroscopic state of the cell, thereby improving the performance of the cell.
2. The electron current density of the corrugated electrolyte cell is larger than that of the flat electrolyte cell, but the triangular corrugated electrolyte increases the difficulty of electron transport inside the cell due to its large number of corrugations, resulting in its electron current density being lower than that of the other two corrugated electrolyte cells. In addition, due to the smaller cathode thickness, the ratio of air channel width to cathode thickness is large, which reduces the resistance of electron transport in the cathode, so the electron current density of the cathode is generally greater than that of the anode.
3. The corrugated electrolyte enlarges the active reaction area, so the consumption of hydrogen and oxygen by the cell is increased, resulting in the concentration polarization of the corrugated electrolyte cell being larger than that of the flat electrolyte cell. The rectangular corrugated electrolyte has the largest increase in concentration polarization. This is a negative effect of the introduction of the corrugated electrolyte on the cell, but it does not affect the overall performance of the cell.
4. The introduction of corrugated electrolytes will increase the current density of the cell. In the case of typical operating voltage  $V=0.7$  V, the current density of the cell increases with the expansion coefficient. In a cell with a rectangular corrugated electrolyte, the expansion coefficient  $\lambda=1.47$ , and its current density is relative to the flat electrolyte cell. The current density of 38.01% is improved.

**Data availability** Research data are not shared.

## Declarations

**Conflict of interest** The authors declare no competing interests.

## References

- Konno A, Iwai H, Saito M, Yoshida H (2011) A corrugated mesoscale structure on electrode–electrolyte interface for enhancing cell performance in anode-supported SOFC. *J Power Sources* 196(18):7442–7449. <https://doi.org/10.1016/j.jpowsour.2011.04.051>
- Konno A, Iwai H, Inuyama K, Kuroyanagi A, Saito M, Yoshida H, Kodani K, Yoshikata K (2011) Mesoscale-structure control at anode/electrolyte interface in solid oxide fuel cell. *J Power Sources* 196(1):98–109. <https://doi.org/10.1016/j.jpowsour.2010.07.025>
- Xie J, Hao W, Wang F (2019) Crack propagation of planar and corrugated solid oxide fuel cells during cooling process. *Int J Energy Res* 43(7):3020–3027. <https://doi.org/10.1002/er.4369>
- Cebollero JA, Lahoz R, Laguna-Bercero MA, Larrea A (2017) Tailoring the electrode–electrolyte interface of solid oxide fuel cells (SOFC) by laser micro–patterning to improve their electrochemical performance. *J Power Sources* 360:336–344. <https://doi.org/10.1016/j.jpowsour.2017.05.106>
- Su PC, Chao CC, Shim JH, Fasching R, Prinz FB (2008) Solid oxide fuel cell with corrugated thin film electrolyte. *Nano Lett* 8(8):2289–2292. <https://doi.org/10.1021/nl800977z>
- Chao CC, Hsu CM, Cui Y, Prinz FB (2011) Improved solid oxide fuel cell performance with nanostructured electrolytes. *ACS Nano* 5(7):5692–5696. <https://doi.org/10.1021/nn201354p>
- Chesnaud A, Delloro F, Geagea M, Abellard AP, Ouyang J, Li D, Shi T, Chi B, Ihringer R, Cassir M, Thorel A (2017) Corrugated electrode/electrolyte interfaces in SOFC: theoretical and experimental development. *Solid Oxide Fuel Cells* 15 (Sofc-Xv) 78(1):1851–1863. <https://doi.org/10.1149/07801.1851ecst>
- Delloro F, Viviani M (2012) Simulation study about the geometry of electrode–electrolyte contact in a SOFC. *J Electroceram* 29(3):216–224. <https://doi.org/10.1007/s10832-012-9766-8>
- Otake T, Yokoyama M, Nagai K, Ukai K, Mizutani Y (2007) Effect of GDC electrolyte thickness on the performance of anode supported micro tubular SOFC [Proceedings Paper]. *Solid Oxide Fuel Cells* 10 (SOFC-X), PTS 1 AND 2
- Jia J, Shen S, Riffat SB, Gillott M (2005) Structural parameters study of a tubular solid oxide fuel cell [Article]. *J Energy Inst* 78(2):76–80. <https://doi.org/10.1179/174602205X39803>
- Subotić V, Stoeckl B, Lawlor V, Strasser J, Schroettner H, Hochenauer C (2018) Towards a practical tool for online monitoring of solid oxide fuel cell operation: an experimental study and application of advanced data analysis approaches. *Appl Energy* 222:748–761. <https://doi.org/10.1016/j.apenergy.2018.03.182>
- Liu S, Kong W, Lin Z (2009) A microscale modeling tool for the design and optimization of solid oxide fuel cells. *Energies* 2(2):427–444. <https://doi.org/10.3390/en20200427>
- Andersson M, Paradis H, Yuan J, Sundén B (2013) Three dimensional modeling of an solid oxide fuel cell coupling charge transfer phenomena with transport processes and heat generation. *Electrochim Acta* 109:881–893. <https://doi.org/10.1016/j.electacta.2013.08.018>
- Todd B, Young JB (2016) Thermodynamic and transport properties of gases for use in solid oxide fuel cell modelling (vol 110, pg 186, 2002). *J Power Sources* 320:349–349. <https://doi.org/10.1016/j.jpowsour.2016.04.123>
- Khazaei I, Rava A (2017) Numerical simulation of the performance of solid oxide fuel cell with different flow channel geometries. *Energy* 119:235–244. <https://doi.org/10.1016/j.energy.2016.12.074>
- Li J, Kong W, Lin Z (2013) Theoretical studies on the electrochemical and mechanical properties and microstructure optimization of micro-tubular solid oxide fuel cells. *J Power Sources* 232:106–122. <https://doi.org/10.1016/j.jpowsour.2013.01.006>
- Lee S, Kim H, Yoon KJ, Son J-W, Lee J-H, Kim B-K, Choi W, Hong J (2016) The effect of fuel utilization on heat and mass transfer within solid oxide fuel cells examined by three-dimensional numerical simulations. *Int J Heat Mass Transf* 97:77–93. <https://doi.org/10.1016/j.ijheatmasstransfer.2016.02.001>
- Serincan MF, Pasaogullari U, Singh P (2020) Controlling reformation rate for a more uniform temperature distribution in an internal methane steam reforming solid oxide fuel cell. *J Power Source* 468. <https://doi.org/10.1016/j.jpowsour.2020.228310>
- Celik AN (2018) Three-dimensional multiphysics model of a planar solid oxide fuel cell using computational fluid dynamics approach. *Int J Hydrogen Energy* 43(42):19730–19748. <https://doi.org/10.1016/j.ijhydene.2018.08.212>
- Fu P, Yang J, Wang Q (2020) Numerical study on mass transfer and electrical performance of anode-supported planar solid oxide fuel cells with gradient porosity anode. *J Heat Trans* 142(2). <https://doi.org/10.1115/1.4045304>
- Chaudhary TN, Saleem U, Chen B (2019) Reacting flow coupling with thermal impacts in a single solid oxide fuel cell. *Int J Hydrogen Energy* 44(16):8425–8438. <https://doi.org/10.1016/j.ijhydene.2019.02.043>
- Chan SH, Xia ZT (2001) Anode micro model of solid oxide fuel cell. *J Electrochem Soc* 148(4). <https://doi.org/10.1149/1.1357174>
- Ni M, Leung MKH, Leung DYC (2007) Micro-scale modelling of solid oxide fuel cells with micro-structurally graded electrodes. *J Power Sources* 168(2):369–378. <https://doi.org/10.1016/j.jpowsour.2007.03.005>
- Tseronis K, Fragkopoulou IS, Bonis I, Theodoropoulos C (2016) Detailed multi-dimensional modeling of direct internal reforming solid oxide fuel cells. *Fuel Cells* (Weinh) 16(3):294–312. <https://doi.org/10.1002/fuce.201500113>
- Wang Y, Zhan R, Qin Y, Zhang G, Du Q, Jiao K (2018) Three-dimensional modeling of pressure effect on operating characteristics and performance of solid oxide fuel cell. *Int J Hydrogen Energy* 43(43):20059–20076. <https://doi.org/10.1016/j.ijhydene.2018.09.025>
- Janardhanan VM, Deutschmann O (2006) CFD analysis of a solid oxide fuel cell with internal reforming: coupled interactions of transport, heterogeneous catalysis and electrochemical processes. *J Power Sources* 162(2):1192–1202. <https://doi.org/10.1016/j.jpowsour.2006.08.017>
- Li Y, Yan H, Zhou Z, Wu WT (2019) Three-dimensional nonisothermal modeling of solid oxide fuel cell coupling electrochemical kinetics and species transport. *Int J Energy Res*. <https://doi.org/10.1002/er.4707>
- Ferguson JR, Fiard JM, Herbin R (1996) Three-dimensional numerical simulation for various geometries of solid oxide fuel cells. *J Power Source* 58(2):109–122. [https://doi.org/10.1016/0378-7753\(95\)02269-4](https://doi.org/10.1016/0378-7753(95)02269-4)
- Seo H, Kishimoto M, Ding C, Iwai H, Saito M, Yoshida H (2020) Improvement in the electrochemical performance of anode-supported solid oxide fuel cells by meso- and nanoscale structural modifications. *Fuel Cells* 20(5):570–579. <https://doi.org/10.1002/fuce.202000079>
- Pesce A, Hornés A, Núñez M, Morata A, Torrell M, Tarancón A (2020) 3D printing the next generation of enhanced solid oxide fuel and electrolysis cells. *J Mater Chem A* 8(33):16926–16932. <https://doi.org/10.1039/d0ta02803g>



31. Li TS, Xu C, Chen T, Miao H, Wang WG (2010) Chlorine contaminants poisoning of solid oxide fuel cells. *J Solid State Electrochem* 15(6):1077–1085. <https://doi.org/10.1007/s10008-010-1166-x>
32. Liu P, Fan S, Liu Y, Han X, Jin Z (2021) Three-dimensional modeling of anode-supported planar SOFC with corrugated electrolyte. *J Electrochem Soc* 168(10). <https://doi.org/10.1149/1945-7111/ac2974>

**Publisher's Note** Springer Nature remains neutral with regard to jurisdictional claims in published maps and institutional affiliations.

Springer Nature or its licensor (e.g. a society or other partner) holds exclusive rights to this article under a publishing agreement with the author(s) or other rightsholder(s); author self-archiving of the accepted manuscript version of this article is solely governed by the terms of such publishing agreement and applicable law.